Point-by-point responses to second review of "The Role of Ice Nuclei Recycling in the Maintenance of Cloud Ice in Arctic Mixed-Phase Stratocumulus" by Amy Solomon, Graham Feingold and Matthew Shupe

Thank you to both the Editor and Reviewer #1 for these comments. We hope you find the point-by-point responses below and the revised paper adequately address your concerns. The response to each comment is in blue font.

Response to Editors Comments:

1) In his first major comment, reviewer #2 has asked for clarifications on the implementation of the prognostic IN tracers. Your explanations in lines 260-264 of the replies are illuminative; please add them also to the paper itself.
   These lines have been added to the model description.

2) Reviewer #2 also asked for clarifications on the value of 5.8/liter. I think your explanations on this important point should be further expanded. In the manuscript, you have added text from line 806 onwards which reveals that the initial N_IN is a sum over all bins, i.e. it equals N_IN given by eq. (2) evaluated at the temperature the coldest bin (-20.2°C). Please state so explicitly in the text. Also, please add what the temperature range for the IN bins was based on. (See also the related question by reviewer #1). According to Fig. 1, the temperature does not reach down to -20.2°C in the initial profile – does is decrease to this value later in the simulation?
   The text has been changed to read "In a discrete bin formulation this results in 3.26 L^{-1} in the warmest bin and 0.23 L^{-1} additional IN that are available for nucleation in the coldest bin, resulting in N_IN given by eq. (2) evaluated at the temperature the coldest bin (-20.2°C)". The value of -20.2 ^{o}C for the coldest bin was chosen because this is coldest temperature that is reached in the cloud layer during the integration. The temperature of the mixed layer continually cools due to cloud top cooling (see Figure 7).

3) Check the page numbers for Abdul-Razzak & Ghan in the reference list.
   Thank you, the page numbers have been corrected.

4) Reference Cziczo et al: Saatho -> Saathoff
   Thank you, the reference has been corrected.

Response to Reviewer #1 Second Review:

1 General Comments

The authors have successfully addressed the concerns presented after the first round of reviews. Because the manuscript is fairly abundant with information, it is clear that the authors made satisfactory attempts to clarify any uncertainties that the reader may have. My recommendation for this manuscript is accept for publication after considering the minor comments below.

Thank you very much for reading the paper so carefully and for your constructive comments.

2 Specific Comments

1) Line 725, “with” should be “, which”
   Text corrected.

2) Line 790, The authors may consider editing this sentence to read “Therefore, additional IN become available for activation with decreasing temperature and as the cloud layer cools” so as to imply that a cooler portion of the cloud would activate more IN according to Fig. 2. Also, the cloud layer in Fig. 1 suggests that IN would only be activated near cloud top, at least initially, as the cloud base extends to temperatures warmer than the threshold temperature bins in Fig. 2. Perhaps this is only a consequence of model spin-up.
   Text changed as suggested. Yes, this is correct about the initial activation at cloud top. Yes, this is a consequence of model spin-up.

3) Lines 809-10, “..additional IN that are available for nucleation in the coldest bin”: The temperature of the coldest bin in Fig. 2 falls below the minimum temperature of the cloud layer in Fig. 1, so perhaps this result is only valid once the layer temperature drops? Additionally, in the following sentence, should it be assumed that the “first bin” corresponds to the warmest temperature?
   Yes, this is correct. The value of -20.2 ^{o}C for the coldest bin was chosen because this is coldest temperature that is reached in the cloud layer during the integration. The temperature of the mixed layer continually cools due to cloud top cooling (see Figure 7).

4) Line 888, I believe “cloud layer” should be replaced with “mixed layer”.
   The text has been changed as suggested.

5) Line 959: “buffering” is not yet a common term and should be defined.
   The sentence has been changed to read, “…for additional negative or “buffering” feedbacks”

6) Figure 2 caption, “IN increments...at colder temperatures”: This sentence is unclear. What is meant by IN increments between lines? An example of this may help. Also, are the ”colder temperatures” those below -15, or colder?
   The sentence has been changed to read, “Note additional IN become available for nucleation at colder temperatures, such that, for example, at -20.2^{o}C (the coldest temperature in the Control simulation) the total number of IN available for activation is ~1.5 L^{-1}”.

7) Figure 5: Is it safe to say that the autoconversion threshold from ice to snow is 0.7 mm? Are ice results throughout (e.g. IWP, etc.) the paper for ice only, or do they include snow? If ice only, are the IN that are activated as ice then converted to snow considered lost?
   I am using the Morrison microphysics and the autoconversion threshold from ice to snow is set to 0.125 mm. IWP includes both ice and snow.

8) Figure 7: Perhaps consider changing the colorbar in (D) so that > 100% and < 35% are not both white.

Changed as suggested.

9) Figure 9: [1] N_{NI} on line 1510 should be N_{ICE}. [2] It appears there are extra black lines in the legends of (A) and (B) in front of "Activation" and "Precipitation," respectively. [3] Should the red line in the legend of (B) read turbulence? [4] Are all the results in (B) at cloud base or does this only apply to precipitation? If the former, perhaps change the title to "IN Flux at cloud base".
N_NI changed to N_ICE. The black lines in (A) and (B) are minus signs. The legend in (B) has been corrected (and thank you for catching this). In (B) both turbulence and precipitation are evaluated at cloud base. The legend has been changed to make this clear. The title has not been changed because sublimation is not evaluated at cloud base.

10) All figures: Please consider adding a white background to all the figure legends.
Thank you but we feel the figures are clearer with legends without white backgrounds.

The Role of Ice Nuclei Recycling in the Maintenance of Cloud Ice in Arctic Mixed-Phase Stratocumulus

Amy Solomon[12], Graham Feingold[2], and Matthew D. Shupe[12]

(1) Cooperative Institute for Research in Environmental Sciences, University of Colorado Boulder, Boulder, Colorado, USA.

(2) Earth System Research Laboratory, National Oceanic and Atmospheric Administration, Boulder, Colorado, USA.

Corresponding author: Amy Solomon, NOAA/ESRL, PSD3, 325 Broadway, Boulder, Colorado 80305-3337, USA. (amy.solomon@noaa.gov)

September 12, 2015

Abstract

This study investigates the maintenance of cloud ice production in Arctic mixed phase stratocumulus in large eddy simulations that include a prognostic ice nuclei (IN) formulation and a diurnal cycle. Balances derived from a mixed-layer model and phase analyses are used to provide insight into buffering mechanisms that maintain ice in these cloud systems. We find that for the case under investigation, IN recycling through subcloud sublimation considerably prolongs ice production over a multi-day integration. This effective source of IN to the cloud dominates over mixing sources from above or below the cloud-driven mixed layer. Competing feedbacks between dynamical mixing and recycling are found to slow the rate of ice lost from the mixed layer when a diurnal cycle is simulated. The results of this study have important implications for maintaining phase partitioning of cloud ice and liquid that determine the radiative forcing of Arctic mixed-phase clouds.

1 Introduction

Reliable climate projections require realistic simulations of Arctic cloud feedbacks. Of particular importance is accurately simulating Arctic mixed-phase stratocumuli (AMPS), which are ubiquitous and play an important role in regional climate due to their impact on the surface energy budget and atmospheric boundary layer structure through cloud-driven turbulence, radiative forcing, and precipitation (Curry et al., 1992; Walsh and Chapman, 1998; Intrieri et al., 2002; Shupe and Intrieri, 2004; Sedlar et al., 2011; Persson, 2012). For example, Bennartz et al. (2012) showed that the extreme melt events observed at Summit, Greenland in July 2012 would not have occurred without the surface radiative forcing produced by AMPS.

AMPS are characterized by a liquid cloud layer with ice crystals that precipitate from cloud base even at temperatures well below freezing (Hobbs and Rangno, 1998; Intrieri et al., 2002; McFarquhar et al., 2007). Radiative cooling near cloud top generates turbulence that maintains the liquid layer and forms an approximately well-mixed layer that extends as far as 500 meters below cloud base. These cloud-driven mixed layers are frequently decoupled from the surface layer, limiting the impact of fluxes of heat, moisture, and aerosols on the cloud layer from below (Solomon et al., 2011; Shupe et al., 2013). However, unlike subtropical cloud-topped boundary layers where decoupling enhances cloud breakup by cutting the cloud system off from the surface source of moisture, decoupled AMPS can persist for extended periods of time due to weak precipitation fluxes out of the mixed layer and relatively moist air entrained into the cloud layer at cloud top (Tjernström et al., 2004; Solomon et al., 2011; Sedlar et al., 2012; Solomon et al., 2014).

AMPS are challenging to model due to uncertainties in ice microphysical processes that determine phase partitioning between ice and radiatively important cloud liquid water (Sandvik et al., 2007; Tjernström et al., 2008; Klein et al., 2009, Karlsson and Svensson, 2011; Barton et al., 2012; Birch et al., 2012; de Boer et al., 2012), which drives turbulence that maintains the system. Phase partitioning depends upon the number, shape, and size of ice crystals, since these determine the efficiency of water vapor uptake by ice and hence the availability of water vapor for droplet formation (Chen and Lamb, 1994; Sheridan et al., 2009; Ervens et al., 2011; Hoose and Möhler, 2012).

Since temperatures in AMPS are too warm for homogenous ice nucleation, ice must form through heterogeneous nucleation. Aerosols with properties to serve as seeds for heterogeneous ice crystal formation are referred to as ice nuclei (IN). A number of different aerosols such as mineral dust (Broadley et al., 2012; Kulkarni et al., 2012; Lüönd et al., 2010; Möhler et al. 2006; Pinti et al., 2012; Welti et al., 2009), soot (DeMott, 1990), sea salts (Wise et al., 2012), and bacteria (Kanji et al., 2011; Levin and Yankofsky, 1983) have been observed to act as IN, all of which nucleate at different temperatures and supersaturation ranges. In addition, observations indicate that nucleation properties are modified by aging and coating of aerosols (Möhler et al., 2005; Cziczo et al. 2009). Heterogeneous ice nucleation can occur by a number of modes: either in the presence of super-cooled droplets, when an aerosol comes into contact with a droplet (contact freezing), is immersed in a droplet (immersion freezing), or by vapor deposition on IN (deposition freezing) (Pruppacher and Klett, 1997).

171 IN can be entrained into the cloud-driven mixed layer through turbulent mixing from above
172 and/or below. Recent studies indicate that entrainment alone cannot account for observed ice
173 crystal number concentration (N_{ICE}) (Fridlind et al., 2012), motivating the use of diagnostic
174 formulations for ice formation to produce model simulations of AMPS with realistic phase
175 partitioning (Ovchinnikov et al., 2011). While this modeling strategy constrains N_{ICE} to be
176 close to the measured values it eliminates the dynamical-microphysical feedbacks that
177 regulate ice/liquid phase partitioning (Avramov et al., 2011).

178 Here we investigate a relatively unexplored source of ice production--recycling of ice
179 nuclei in regions of ice subsaturation. AMPS frequently have ice-subsaturated air near the
180 cloud-driven mixed-layer base where falling ice crystals can sublimate, leaving behind IN.
181 This feedback loop is referred to hereon as "recycling". Recycling was found to be
182 significant in large eddy simulations of a single-layer stratocumulus observed during the
183 Department of Energy Atmospheric Radiation Measurement Program's Mixed-Phase Arctic
184 Cloud Experiment (M-PACE; Verlinde et al., 2007; Fan et al., 2009). AMPS observed during
185 M-PACE formed due to a cold-air outbreak, where large fluxes of heat and moisture over the
186 open ocean forced turbulent roll clouds that were coupled to the surface layer. This coupling
187 with the surface layer prevented the identification of the role of dynamics internal to the
188 cloud-driven mixed layer in maintaining phase-partitioning.

189 In this study we focus on the internal microphysics and dynamics of the cloud-driven mixed
190 layer by investigating processes in an AMPS decoupled from surface sources of moisture,
191 heat, and ice nuclei. We posit that recycling plays a significant role more generally since, for
192 example, assuming an adiabatic vertical profile, a 650 meter-deep mixed layer with a cloud-

top temperature of -16°C requires a water vapor mixing ratio of at least 1.7 g kg^{-1} at mixed-layer base to be saturated with respect to ice, i.e., in order for recycling to be a *negligible* source of ice nuclei in the mixed layer. This value is typically only seen in the Arctic between May-September (Serreze et al., 2012), while persistent AMPS frequently occur outside of these months (Shupe et al., 2011).

We examine the role of IN recycling in maintaining ice production using large eddy simulations of a springtime decoupled AMPS. Three simulations are analyzed; a "Control" with recycling turned on and shortwave radiation turned off (to compare with previous simulations of this case that use different IN formulations and shortwave radiation turned off), "NoRecycle" with IN recycling turned off to identify the impact of recycling on the cloud life-time and phase partitioning, and "SW" with recycling and shortwave radiation turned on to identify the impact of realistic diurnal heating and cooling tendencies on the recycling process. This study builds on previous studies of this case, all of which exclude shortwave radiation (Avramov et al., 2011; Solomon et al., 2011, 2014), by including a prognostic equation for IN and a diurnal cycle. Within this modeling framework we investigate the relative roles of recycling and entrainment of IN in maintaining cloud ice production.

2 Case Description

The case derives from observations of a persistent single-layer Arctic mixed-phase stratocumulus cloud observed near Barrow, AK on 8 April 2008 during the Indirect and Semi-Direct Aerosol Campaign (McFarquhar et al., 2011) (see Fig. 1). The adjacent Beaufort Sea was generally ice covered during this time, with significant areas of open water observed east of Barrow. A 4-K temperature inversion with inversion base at 1.05 km was observed

via a radiosonde at 17:34UTC; static stability was near neutral within the mixed layer overlaying a stable near-surface layer with static stability greater than 2 K km^{-1} below 500 m. The water vapor mixing ratio, q_v, decreased from 1.7 g kg^{-1} at the surface to 1.2 g kg^{-1} at cloud top, above which a secondary maximum of 1.6 g kg^{-1} was observed. Winds were east-southeasterly throughout the lowest 2 km.

Measurements from ground-based, vertically pointing, 35-GHz cloud radar, micropulse lidar, and dual-channel microwave radiometer at Barrow indicated a mixed-phase cloud layer starting at 8 UTC on 8 April 2008 with a cloud top at approximately 1.5km that slowly descended to approximately 0.5 km over a 26 hour period. At the time of the 17:34 sounding the cloud layer extended into the inversion by 100 m, had a cloud base at 0.9 km, and cloud top at 1.15 km. Cloud ice water path (IWP), derived from cloud radar reflectivity measurements, varied from 20–120 g m^{-2} within 10 min of the sounding, with an uncertainty of up to a factor of 2 (Shupe et al., 2006). Concurrently liquid water path (LWP), derived from dual-channel microwave radiometer measurements, was 39–62 g m^{-2}, with an uncertainty of 20–30 g m^{-2} (Turner et al., 2007).

Research flights were conducted by the National Research Council of Canada Convair-580 at 22:27-23:00 UTC on 8 April 2008 over the ocean northwest of Barrow (McFarquhar et al., 2011). Droplet concentrations measured by a Particle Measuring Systems Forward Scattering Spectrometer Probe varied between 100 and 200 cm^{-3}. Ice crystal number concentrations measured by Stratton Park Engineering Company 2D-S and Particle Measuring Systems 2D-P optical array probes for sizes larger than 100 μm together averaged 0.4 L^{-1}. IN concentrations measured with the Texas A&M Continuous Flow Diffusion Chamber varied

237 from 0.1 L^{-1} to above 20 L^{-1}. Ice crystal habit estimated using the automated habit
238 classification procedure of Korolev and Sussman (2000) indicated primarily dendritic crystal
239 habits.

240 **3 Model Description**

241 We use the large eddy simulation mode of the Advanced Research WRF model (WRFLES)
242 Version 3.3.1 (Yamaguchi and Feingold, 2012) with the National Center for Atmospheric
243 Research Community Atmospheric Model longwave radiation package (Collins et al., 2004),
244 RRTMG shortwave package (Iacono et al., 2008), the Morrison two-moment microphysical
245 scheme (Morrison et al., 2009), and a 1.5-order turbulent kinetic energy prediction scheme
246 (Skamarock et al., 2008). Surface fluxes are calculated uses the modified MM5 similarity
247 scheme which calculates surface exchange coefficients for heat, moisture, and momentum
248 following Webb (1970) and uses Monin-Obukhov with Carlson-Boland viscous sub-layer
249 and standard similarity functions following Paulson (1970) and Dyer and Hicks (1970).

Amy Solomon 9/13/2015 11:34 AM
Deleted: ith

250 All model runs are initialized with winds, temperature, and water vapor from the 17Z 8 April
251 2008 sounding at Barrow, AK (see Fig.1). Initial surface pressure is 1020 hPa. Divergence is
252 assumed to be $2.5\text{x}10^{-6}$ s^{-1} below the temperature inversion and zero above, giving a linear
253 increase in large-scale subsidence from zero at the surface to 2.7 mm s^{-1} at the base of the
254 initial inversion (z=1.1 km). This value for divergence was chosen so that the height of the
255 temperature inversion at cloud top is steady. The divergence used in this study is smaller than
256 the divergence used in the WRFLES study of the same case by Solomon et al. (2014) due to

258 the reduced LWPs in this current study and therefore reduced turbulent entrainment that
259 balances large-scale subsidence in a steady simulation.

260 All simulations are run on a domain of 3.2 × 3.2 × 1.8 km with a horizontal grid spacing of
261 50 m and vertical spacing of 10 m. The domain has 65(x)×65(y)×180(z) gridpoints and is
262 periodic in both the x- and y-directions. The top of the domain is at 1.8 km, which is 0.7 km
263 above cloud top in this case. The model time step is 0.75 s. The structure of the cloud layer is
264 insensitive to changes in resolution and domain size. For example, tests run for Solomon et al.
265 (2014) demonstrated that increasing the vertical and horizontal resolutions by a factor of two
266 resulted in an increase in LWP and IWP by 5% and 1%, respectively, while increasing the
267 domain size by a factor of two in both the x- and y-directions results in an increase in LWP
268 and IWP of less than 1%.

269 Cloud droplets are activated using resolved and subgrid vertical motion (Morrison and Pinto
270 2005) and a log-normal aerosol size distribution (assumed to be ammonium bisulfate and
271 30% insoluble by volume) to derive cloud condensation nuclei spectra following Abdul-
272 Razzak and Ghan (2000). The aerosol accumulation mode is specified with concentrations of
273 165 cm^{-3}, modal diameter of 0.2 μm, and geometric standard deviation of 1.4 μm, based on in
274 situ ISDAC measurements. In this formulation, IN and cloud condensation nuclei are treated
275 as separate species.

276 Temperature and moisture profiles are nudged to the initial profiles in the top 400 m of the
277 domain with a time scale of 1 hour. The model is initialized with winds, temperature, and
278 water vapor similar to the Control integration from Solomon et al. (2014). Horizontal winds

279 are nudged to the initial profiles at and above the initial inversion base with a timescale of 2
280 hours. Initial temperature and subgrid turbulent kinetic energy (TKE) are perturbed below the
281 top of the mixed layer with pseudo-random fluctuations with amplitudes of +/- 0.1 K and 0.1
282 $m^2\ s^{-2}$, respectively. The liquid layer is allowed to form in the absence of ice during the first
283 hour of the integration to prevent potential glaciation during spinup.

284 The cloud-driven mixed layer is defined as the region where the liquid-ice water static energy
285 is approximately constant with height. We define the boundaries of the mixed-layer top and
286 base to occur where the slopes of liquid-ice static energy exceed $7x10^{-3}$ K m^{-1} and $1x10^{-3}$ K
287 m^{-1}, respectively. Cloud top and base are defined as the heights where cloud water mixing
288 ratio, q_c, is equal to $1x10^{-4}$ g kg^{-1}.

289 Nested Weather Research and Forecasting (WRF) model simulations of this case performed
290 with an inner grid at LES resolution (Solomon et al. 2011) demonstrate that moisture is
291 provided to the cloud system by a total water inversion at cloud top and that the mixed layer
292 does not extend to the surface, i.e., the mixed layer is largely decoupled from surface sources
293 of moisture. In addition, the nested simulations indicate that cloud liquid water, q_c, is
294 maintained within the temperature inversion by downgradient turbulent fluxes of q_v from
295 above and direct condensation driven by radiative cooling. These processes cause at least
296 20% of q_c to extend into the temperature inversion.

297 WRFLES has been modified to include a prognostic equation for IN number concentration
298 (N_{IN}),

$$\frac{\partial N_{IN}}{\partial t} + ADV + DIFF = \frac{\delta N_{IN}}{\delta t}\Big|_{activation} + \frac{\delta N_{IN}}{\delta t}\Big|_{sublimation} \quad (1)$$

where ADV represents advection and DIFF represents turbulent diffusion. Activation is also referred to as nucleation of ice and sublimation is also referred to as recycling of IN.

Here we adopt an empirical approach by initializing N_{IN} with an observationally based relationship expressing the number of available IN as a function of temperature in regions of water-saturation (DeMott et al., 2010),

$$N_{IN} = \mathrm{F} * 0.117 \exp\left(-0.125 * (\mathrm{T} - 273.2)\right) \quad (2)$$

where F is an empirically derived scale factor and T is temperature in Kelvin. Sixteen prognostic equations are integrated for N_{IN} in equally spaced temperature intervals with nucleation thresholds between -20.2°C and -15.5°C (see Fig. 2). Therefore, additional IN become available for activation with decreasing temperature and as the cloud layer cools. IN number concentrations are initially specified using equation 2, such that the initial IN in bin *k* is equal to the number of IN calculated by equation 2 at the threshold temperature *k + 1* minus that calculated at temperature *k*. After the initial time 50% of the IN available in a bin nucleates if the in-situ temperature is above the threshold temperature and the local conditions exceed water saturation. Therefore, initial N_{IN} concentrations are a function of the nucleation threshold temperatures and are independent of the in-situ temperature. The in-situ temperature in regions of water saturation determines how many IN are activated. Due to the pristine dendritic nature of the observed crystals, ice shattering and aggregation are neglected in the simulations and sublimation returns one N_{IN} per crystal.

Amy Solomon 9/13/2015 12:02 PM
Formatted: Space After: 12 pt, Tabs: 0.15", Left + 0.5", Left

Amy Solomon 9/13/2015 11:55 AM
Deleted: Therefore, additional IN become available for activation as the cloud layer cools

Amy Solomon 9/13/2015 12:01 PM
Formatted: Font:(Default) Times New Roman

Amy Solomon 9/13/2015 12:01 PM
Formatted: Font:(Default) Times New Roman

Amy Solomon 9/13/2015 12:01 PM
Formatted: Font:(Default) Times New Roman

Amy Solomon 9/13/2015 12:01 PM
Formatted: Font:(Default) Times New Roman

Amy Solomon 9/13/2015 12:01 PM
Formatted: Font:(Default) Times New Roman

Amy Solomon 9/13/2015 12:01 PM
Formatted: Font:(Default) Times New Roman

Amy Solomon 9/13/2015 12:02 PM
Deleted: I

Amy Solomon 9/13/2015 12:02 PM
Deleted: . To take deviations from the empirical derivation into account, IN are activated with 50% efficiency (by multiplying the activation tendency in equation (1) by 0.5), however results are insensitive to this parameter (not shown)

N_{IN} (in units of L^{-1}) integrated over the domain in each temperature bin k at time t is equal to

$$\overline{N}_{IN}(k,t) = \iiint N_{IN}(x,y,z,k,t)\ dx\ dy\ dz. \quad (3)$$

Upon sublimation, the modification of activation thresholds that can occur for previously nucleated IN, i.e. preactivation (Roberts and Hallett, 1967), is not considered and N_{IN} are returned to each bin k with weighting

$$W_k = [\overline{N}_{IN}(k,0) - \overline{N}_{IN}(k,t)\ ]/\ \overline{N}_{IN}(k,0) \quad (4)$$

where W_k is normalized such that $\sum W_k = 1$. The W_k are recalculated each time step. In this way, IN are recycled preferentially to each of the 16 temperature bins from which they originated (Feingold et al., 1996).

The factor F in Eq. (2) is set to 4 for all simulations yielding an initial N_{IN} summed over all bins at every gridpoint equal to 5.8 L^{-1}, compared to 10 L^{-1} used in LES studies of the same case presented in Avramov et al. (2011). In a discrete bin formulation this results in 3.26 L^{-1} in the warmest bin and 0.23 L^{-1} additional IN that are available for nucleation in the coldest bin, resulting in N_{IN} given by eq. (2) evaluated at the temperature the coldest bin (-20.2°C). Given the initial temperatures in the cloud layer, all IN from the first bin in the cloud layer nucleate. This causes an initial spike in cloud ice number concentration, which also causes a large precipitation flux out of the mixed layer. It takes approximately 6 hours for the cloud layer to reach a quasi-equilibrium with steady cloud ice production. Supplementary integrations were done to test for robustness of the results presented in Section 4 by varying initial IN concentrations, i.e., the factor F, (shown in Fig. 3) and by varying snow density and

Amy Solomon 9/13/2015 12:53 PM
Deleted: n

345 fall speeds (shown in Fig. 4). Fig. 3 shows that the simulation maintains ice production when
346 the initial N_{IN} is increased or decreased by ~3 L^{-1} relative to Control. Fig. 4 shows that the
347 simulations maintain quasi-steady ice and liquid water paths after an initial spinup but the
348 amount of ice produced is sensitive to the snow fall speed.

349 Crystal size distributions for averaged values of ice water mixing ratio and number
350 concentration from the Control integration are shown in Fig. 5. These crystal size
351 distributions are consistent with the Avramov et al. (2011) simulations of this case where
352 crystal habits are assumed to be high-density pristine dendrites. The distribution shown in Fig.
353 5 underestimates the number of large (greater than 5mm) crystals as estimated by the 2D-S
354 and 2D-P probes (see Avramov et al. (2011) for a detailed discussion of the measurements).

355 The Control integration is run with shortwave radiation turned off in order to compare with
356 previous LES studies of this case (Avramov et al. 2011; Solomon et al. 2014). The results of
357 Control are compared to two additional simulations; one with IN recycling turned off
358 (hereafter "NoRecycle") and one with recycling and shortwave radiation both turned on
359 (hereafter "SW"). SW is used to investigate how the diurnal cycle impacts IN recycling and
360 ice formation. All runs use the same setup except SW has subsidence reduced by 30% to
361 keep the mixed-layer top from lowering appreciably because of smaller LWPs. This allows
362 for direct comparisons of mixed layer structure and fluxes at the mixed layer boundaries. The
363 NoRecycle run is started from the Control run at hour 6 to prevent the two simulations from
364 diverging due to spinup. The first six hours of integration are not used in the analysis to allow
365 for the spinup of cloud ice. Hours 6-40 are used for analysis of the Control and NoRecycle

simulations and hours 16-76 are used for analysis of the SW simulation to allow for multiple diurnal cycles.

4 Model Results

4.1 Control Integration

In the quasi-steady Control integration, the mixed-layer depth is approximately 850 m and comprises a 375 m deep mixed-phase cloud layer (henceforth "the cloud layer"), extending above the mixed-layer top by 25 m, and a 500 m subcloud layer below (Fig. 6). IN are produced by sublimation of ice crystals below the cloud layer, advected to the cloud layer by turbulence, and activated as ice crystals (Fig. 6). Ice that forms in the cloud layer is transported vertically by turbulence, precipitates to cloud base and below, and sublimates below the cloud layer. At the mixed-layer base, an increase in N_{ICE} due to precipitation approximately balances a decrease in N_{ICE} due to sublimation. These processes constitute a feedback through which ice production and IN recycling are closely related. This feedback between ice production and IN in the mixed layer is linked to dynamic-thermodynamic tendencies, which sustain a subsaturated subcloud layer because the decrease in relative humidity due to an upward turbulent vapor flux exceeds the increase due to sublimation.

The time evolution of horizontally-averaged IN advection plus subsidence (Fig. 7a) shows that the majority of IN activate at cloud base, which is a bit warmer than cloud top but is sufficiently cold to activate many of the IN. However, IN from bins with colder threshold temperatures are advected higher into the cloud where they activate at their threshold temperature. A secondary maximum is seen at cloud top where the coldest temperatures are

found. Also, it is seen that IN are advected into the cloud layer at cloud top for the first 15-18 hours, but this source of IN decreases as IN in the upper entrainment zone are depleted. The turbulent mixing of snow and ice in the mixed-phase cloud layer is clearly seen in Fig. 7b, where ice plus snow number concentrations are well-mixed in the cloud layer. Given the efficient mixing by the turbulent eddies, it is not possible to identify whether ice has nucleated at cloud base or cloud top from the ice number concentrations alone. Fig. 7 also shows the time-height cross sections of horizontally-averaged water vapor mixing ratio and relative humidity with respect to ice. These figures show that the continuous drying and cooling of the mixed layer results in continuous sublimation in the subcloud layer.

LWP and IWP remain steady until hour 16 of the simulation, and decrease slowly thereafter (solid lines in Fig. 8a). LWP and IWP magnitudes are within the observational estimates for this case. In addition, the cloud system is sustained over a multi-day period similar to measurements taken during ISDAC. Continuous cloud-top cooling causes the minimum horizontally-averaged temperature (near cloud top) to decrease from -17.5^{o}C to -20^{o}C from hour 10 to hour 40 (Fig. 8b).

Over the 40-hour integration, the mixed layer remains decoupled from the surface (Fig. 8c). However, this does not prevent the number concentration of ice crystals (N_{ICE}) in the cloud layer from remaining relatively steady, decreasing from vertically integrated values of 372 to 365 m L^{-1} (Fig. 8d, or in terms of vertically averaged cloud layer values, 1.2 L^{-1} to 1.1 L^{-1}). By contrast, while N_{ICE} is maintained in the cloud layer, N_{IN} in the subcloud layer decreases significantly from 2 L^{-1} to 0.2 L^{-1} over the same period. Therefore, even though more N_{ICE} are lost from the cloud than are activated (Fig. 9a), the relatively constant flux of IN into the

Amy Solomon 9/13/2015 1:44 PM
Deleted: cloud

410 cloud layer (Fig. 9b) allows N_{ICE} in the cloud to decrease at a slower rate than N_{IN} in the
411 subcloud layer. The continuous loss of N_{IN} in the subcloud layer is due to the IN flux into the
412 cloud layer exceeding the N_{IN} gained through sublimation and turbulent advection at mixed-
413 layer base (Fig. 9b). This loss is not mitigated by entrainment at mixed-layer top, which is
414 found to be negligible (Fig. 9c), consistent with Fridlind et al. (2011).

415 The feedback loops discussed above are illustrated by the conceptual diagram in Fig. 10,
416 where any change to one link in the cycle leads to an increase or decrease in ice production.
417 For example, a decrease in the turbulent advection of N_{IN} into the cloud layer, slows the
418 activation of IN, reduces the precipitation flux into the subcloud layer, reducing sublimation
419 and availability of IN below cloud base. Both dynamics and thermodynamics play a role in
420 the buffering aspect of these feedback loops since, for example, the slowing of IN activation
421 in the example above would lead to increased cloud liquid production, cloud-top radiative
422 cooling, and enhanced turbulent mixing, which would lead to increased transport of IN into
423 the cloud layer and therefore increased activation of IN.

424 ***4.2 Impact of turning off recycling***

425 When IN recycling is turned off, all IN that activate are lost from the system. This results in a
426 more rapid loss of IN, a decrease in IWP, and a rapid increase in LWP (Fig. 8a,d, dashed
427 lines), in contrast to the measurements that show a steady liquid layer and consistent ice
428 production. Increased cloud liquid water when recycling is turned off results in increased
429 radiative cooling at cloud top, which causes the cloud-driven mixed layer to cool more
430 rapidly (Fig. 8b). These results demonstrate the importance of IN recycling in regulating

phase partitioning. The rapid increase in LWP increases cloud-generated turbulence via enhanced radiative cooling and increases the turbulent mixing of IN from the subcloud layer into the cloud layer, contributing to a more rapid depletion of IN relative to the Control integration. This process eventually becomes limited due to depletion of IN in the reservoir below (Fig. 9b). Due to the additional activation of IN as the cloud layer cools, ice production is maintained in the absence of recycling and the activation of IN in the cloud layer exceeds the upward IN flux at cloud base (Fig. 9a,b). However, the diminishing N_{IN} in the subcloud layer limits IN activation and N_{ICE} rapidly decreases in the cloud layer (Fig. 8d).

4.3 Impact of diurnal cycle

A diurnal cycle is added to the Control simulation in order to investigate how the feedback loops identified in the Control and NoRecycle runs are modified with realistic transient heating and cooling tendencies due to variations in incoming shortwave radiation. A question that is addressed in this diurnal simulation is, to what extent is the continuous production of ice in the Control simulation due to the lack of incoming shortwave radiation, which may overestimate the cooling tendencies in the cloud layer, resulting in an overestimate of IN activation? In addition, we investigate whether allowing for a realistic diurnal cycle provides for additional negative or "buffering" feedbacks.

Amy Solomon 9/13/2015 1:45 PM
Deleted: buffering

Adding a diurnal cycle to the Control simulation produces a diurnal peak in downwelling surface shortwave radiation of 510 W m^{-2} and 6 hours of total darkness per day (Fig. 11b). As shortwave radiation increases, the net radiative cooling near cloud top diminishes, which decreases cloud-generated turbulence, decreasing LWP and cloud-layer thickness. In addition,

453 it is seen that the peak daily LWP coincides with zero shortwave radiation when in-cloud
454 turbulence and cloud thickness are largest (Fig. 11a). These values are on the low end but
455 within the measurements for this ISDAC case.

456 Fig. 11a,b shows that LWP and IWP variability is predominantly driven by the diurnal cycle.
457 However, IWP variability is seen to lag LWP by 3-4 hours because as shortwave radiation
458 decreases the cloud layer cools, which increases activation of IN, increasing N_{ICE}, allowing
459 more ice crystals to grow, which increases IWP (Fig. 11a,b). Similar to the Control
460 simulation subcloud N_{IN} decreases at a faster rate than cloud layer N_{ICE}, but allowing for the
461 warming and cooling tendencies in the diurnal cycle results in cloud layer N_{ICE} that decreases
462 40% more slowly than in the Control simulation (Fig. 11c).

463 Precipitation and turbulent mixing of N_{ICE} (hereafter turbulent mixing is referred to as
464 "T_{ICE}") at cloud base are out of phase by 10 hours (Fig. 11d), with turbulence leading
465 precipitation. When shortwave radiation is weak or absent, the increase in N_{ICE} eventually
466 becomes limited by a decreasing turbulent mixing of IN ("T_{IN}") into the cloud layer from
467 below, as recycling slows due to a decrease in N_{ICE} flux from the cloud layer (Fig. 11d,f).
468 When shortwave radiation is strong, reduction in IWP is limited by weaker precipitation
469 losses, and attendant weaker sublimation and IN flux into the cloud layer (Fig. 11d,f).
470 Entrainment of N_{IN} at the mixed-layer top is insignificant throughout the integration (Fig.
471 11e).

472 **5 Analysis from a mixed-layer perspective**

The results discussed in Section 4 can be understood from balances in a well-mixed layer with sources/sinks at the upper and lower boundaries. Total particle concentration (N_{IN}+N_{ICE}) is only changed by fluxes at the mixed-layer boundaries when recycling is allowed. These fluxes are entrainment of N_{IN} at mixed-layer top and turbulent mixing of both N_{ICE} and N_{IN} (T_{ICE} and T_{IN}) and precipitation of N_{ICE} (P) at mixed-layer base. Since there are no sources and sinks of N_{IN}+N_{ICE} within the mixed layer, the horizontally-averaged N_{IN}+N_{ICE} flux ($f(z)$) must vary linearly from mixed-layer base to mixed-layer top (Lilly, 1968; Bretherton and Wyant, 1997). If it is assumed that f at the mixed-layer base is downward (assumed negative in this formulation) and f at the mixed-layer top is negligible (robust assumptions for a scenario where ice is precipitating from the mixed layer and entrainment is weak), then

$$f(z) = R * \frac{H - z}{H - B}, \qquad B \le z \le H \tag{5}$$

where H is the mixed-layer height, B is the mixed-layer base and R is the total N_{IN}+N_{ICE} flux at the mixed-layer base,

$$R = f|_{\text{Mixed-Layer Base}} = [P + T_{ICE} + T_{IN}]_{\text{Mixed-Layer Base}}, \tag{6}$$

and

$$[T_{ICE} + T_{IN}]_{\text{Cloud Base}} \approx [f - P]_{\text{Cloud Base}}. \tag{7}$$

Since $f < 0$, the turbulent flux of N_{IN} into the cloud layer plus the turbulent flux of N_{ICE} into the subcloud layer is always less than precipitation of N_{ICE} at cloud base. In addition, in a

slowly evolving state where $T_{IN}|_{\text{Mixed-Layer Base}} > 0$, total IN flux due to sublimation in the mixed layer, S, can be written as

$$S \approx [P + T_{ICE}]_{\text{Mixed-Layer Base}} - [P + T_{ICE}]_{\text{Cloud Base}} \quad (8a)$$

$$\approx [f - T_{IN}]_{\text{Mixed-Layer Base}} - [f - T_{IN}]_{\text{Cloud Base}} \quad (8b)$$

and since $f|_{\text{Mixed-Layer Base}}$ is downward and $f|_{\text{Mixed-Layer Top}}$ is negligible (eq. 5),

$$S < T_{IN}|_{\text{Cloud Base}} - T_{IN}|_{\text{Mixed-Layer Base}} \quad (8c)$$

$$< T_{IN}|_{\text{Cloud Base}}. \quad (8d)$$

Thus in a well-mixed layer with an upward $T_{IN}|_{\text{Mixed-Layer Base}}$, sublimation is always less than the flux of N_{IN} into the cloud layer.

Based on results from Control, precipitation of N_{ICE} at cloud base is sufficient to balance the upward turbulent flux of N_{IN} (i.e., $|T_{IN}| \gg |T_{ICE}|$ at cloud base). Therefore, in a well-mixed layer with precipitation of N_{ICE} at the mixed-layer base that is larger in magnitude than an upward turbulent N_{IN} flux at the mixed-layer base, and assuming negligible entrainment at the mixed-layer top

$$|P|_{\text{Cloud Base}} > T_{IN}|_{\text{Cloud Base}} > S. \quad (9)$$

However, if all N_{ICE} sublimate in the mixed layer and the upward turbulent flux of N_{IN} dominates at the mixed-layer base then $f > 0$ and

$$T_{IN}|_{\text{Cloud Base}} > |P|_{\text{Cloud Base}} = S, \quad (10)$$

the mixed layer gains $N_{IN}+N_{ICE}$ over time, resulting in a continuously increasing ice production in the cloud layer. In the presence of shortwave radiation (i.e., in the SW simulation), $T_{IN}|_{\text{Cloud Base}}$ is also greater than $|P|_{\text{Cloud Base}}$ after a period of weakened turbulence and weaker precipitation at the mixed-layer base, due to increased activation of N_{IN} due to decreasing shortwave radiation.

If IN entrainment at the mixed-layer top is not negligible then $f(z)$ must be modified to include fluxes at the mixed-layer top and $|f|_{\text{Cloud Base}}$ will increase. If $|f|_{\text{Cloud Base}}$ increases such that $f_{\text{Cloud Base}} < P_{\text{Mixed-Layer Base}}$, then sublimation will exceed $T_{IN}|_{\text{Cloud Base}}$.

This mixed-layer analysis provides a framework to understand the results presented in Section 4. Specifically, sublimation being less than the turbulent flux of IN is seen to be a property of a well-mixed layer where the total flux at mixed-layer base is downward and the total flux at the mixed-layer top is negligible. In the case where the mixed layer is saturated with respect to ice, sublimation is equal to zero and the turbulent flux of IN at the mixed-layer base is less that the turbulent flux of IN at the cloud base, reducing the flux of IN into the cloud layer. The relationships outlined in this section are appropriate for any AMPS with weak entrainment at cloud top, weak large-scale advective fluxes, and net downward fluxes at the mixed-layer base.

6 Analysis of Buffered Feedbacks in SW

520 Phase diagrams highlight the processes involved in ice production when a diurnal cycle is
521 allowed (following the arrows from green to blue to black to red in Fig. 12a,b). When
522 incoming shortwave radiation is a maximum, recycling (sublimation) is seen to be at a
523 minimum. This is counterintuitive since subcloud relative humidity is low at this time, which
524 would be expected to produce increased sublimation. However, due to weak turbulent mixing
525 between the cloud and subcloud layers the net N_{ICE} flux into the subcloud layer is weak,
526 resulting in weak sublimation and recycling. This situation is reversed as shortwave radiation
527 decreases, since increased cloud-top cooling increases cloud-driven turbulent mixing, which
528 allows recycling to increase in the regions of reduced subcloud relative humidity. As is seen
529 in the conceptual diagram (Fig. 10), this then leads to an increased N_{ICE} flux into the
530 subcloud layer (green arrows, Fig. 12). However, N_{ICE} in the cloud layer doesn't begin to
531 increase until activation in the cloud layer exceeds the flux of N_{ICE} into the subcloud layer
532 (green arrows). This cycle is further amplified as shortwave radiation decreases, namely,
533 decreased shortwave radiation increases cloud-driven turbulence, increasing the flux of IN
534 into the cloud layer, increasing the activation of IN, which increases N_{ICE} in the cloud layer
535 and the N_{ICE} flux from the cloud layer into the subcloud layer (blue arrows).

536 When incoming shortwave radiation is a minimum, more N_{IN} are activated because the cloud
537 layer cools. However, again we see that N_{ICE} tendencies due to thermodynamics are buffered
538 by the slowing of turbulence-driven feedbacks due to a thickening of the cloud layer. Thus, a
539 net increase in N_{ICE} in the cloud layer, commensurate with an increased IWP and
540 precipitation (black arrows), is buffered by a decrease in the downward turbulent mixing of
541 N_{ICE}, which reduces recycling, slowing the feedback loop (see Fig. 10). During the morning
542 hours, as the cloud layer warms and thins and ice activation becomes less efficient,

turbulence continues to decline, slowing the recycling feedback process to the point where limited IN fluxes to the cloud layer inhibit ice production and N_{ICE} declines (red arrows).

7 Summary

We have demonstrated that sustained recycling of IN through a drying subcloud layer and additional activation of N_{IN} due to a cooling cloud layer are sufficient to maintain ice production, and regulate liquid production over multiple days in a decoupled AMPS.

This study provides an idealized framework to understand feedbacks between dynamics and microphysics that maintain phase-partitioning in AMPS. In addition, we have shown that modulation of the cooling of the cloud layer and the humidity of the subcloud layer by the diurnal cycle buffers the mixed-layer system from a loss of particles and promotes the persistence of a mixed-phase cloud system. The results of this study provide insight into the mechanisms and feedbacks that may maintain cloud ice in AMPS even when entrainment of IN at the mixed-layer boundaries is weak. While the balance of these processes changes depending upon the specific conditions of the cloud layer, for example whether the cloud layer is coupled to the surface layer, the mechanisms detailed in this paper will manifest to some degree and therefore the current study provides a framework for understanding the role of recycling in maintaining phase-partitioning in AMPS.

Author Contributions:

A.S., G.F., and M.D.S. conceived and designed the experiments; A.S. performed the simulations; A.S., G.F., and M.D.S. analyzed the model results and co-wrote the paper.

Acknowledgements:

The authors acknowledge discussions with Alex Avramov, Chris Cox, Gijs de Boer, Barbara Ervens, and Ann Fridlind, and Takanobu Yamaguchi for developing the software to run WRF as a large eddy simulation. This research was supported by the Office of Science (BER), U.S. Department of Energy (DE-SC0011918) and the National Science Foundation (ARC-1023366).

569 **References**

570 Abdul-Razzak, H. and Ghan, S. J.: A parameterization of aerosol activation 2. Multiple
571 aerosol types, J. Geophys. Res., 105, 6837–6844, 2000.

572 Avramov, A., Ackerman, A. S., Fridlind, A. M., van Diedenhoven, B., Botta, G., Aydin, K.,
573 Verlinde, J., Korolev, A. V., Strapp, J. W., McFarquhar, G. M., Jackson, R., Brooks, S.
574 D., Glen, A., and Wolde, M.: Toward ice formation closure in Arctic mixed-phase
575 boundary layer clouds during ISDAC, J. Geophys. Res., 116, D00T08,
576 doi:10.1029/2011JD015910, 2011.

577 Barton, N. P., Klein, S. A., Boyle, J. S., and Zhang, Y. Y.: Arctic synoptic regimes:
578 Comparing domain wide Arctic cloud observations with CAM4 and CAM5 during
579 similar dynamics, J. Geophys. Res., 117, D15205, doi:10.1029/2012JD017589, 2012.

580 Bennartz, R., Shupe, M., Turner, D., Walden, V., Steffen, K., Cox, C., Kulie, M. S., Miller,
581 N., and Pettersen, C.: July 2012 Greenland melt extent enhanced by low-level liquid
582 clouds, Nature, 496, 83-86, doi:10.1038/nature12002, 2012.

583 Birch, C. E., Brooks, I. M., Tjernström, M., Shupe, M. D., Mauritsen, T., Sedlar, J., Lock, A.
584 P., Earnshaw, P., Persson, P. O. G., Milton, S. F., and Leck, C.: Modeling atmospheric
585 structure, cloud and their response to CCN in the central Arctic: ASCOS case studies,
586 Atmos. Chem. Phys., 12, 3419-3435, doi:10.5194/acp-12-3419-2012, 2012.

587 Bretherton, C. S. and Wyant, M. C.: Moisture transport, lower-tropospheric stability, and
588 decoupling of cloud-topped boundary layers, J. Atmos. Sci., 54, 148-167, 1997.

589 Broadley, S., Murray, B., Herbert, R., Atkinson, J., Dobbie, S., Malkin, T., Condliffe, E., and
590 Neve, L.: Immersion mode heterogeneous ice nucleation by an illite rich powder
591 representative of atmospheric mineral dust, Atmos. Chem. Phys., 12:287{307,

Amy Solomon 9/13/2015 11:17 AM
Deleted: .

593 doi:10.5194/acp-12-287-2012, 2012.
594 Chen, J.-P. and Lamb, D.: The theoretical basis for the parameterization of ice crystal habits:
595 Growth by vapor deposition, J. Atmos. Sci., 51, 1206–1222, doi:10.1175/1520-
596 0469(1994)051<1206:TTBFTP>2.0.CO;2, 1994.
597 Collins, W. D., Rasch, P. J., Boville, B. A., Hack, J. J., McCaa, J. R., Williamson, D. L., and
598 Briegleb, B. P.: Description of the NCAR Community Atmosphere Model (CAM 3.0),
599 NCAR Technical Note, NCAR/TN-464+STR, 226 pp., 2004.
600 Curry, J. and Ebert, E. E.: Annual cycle of radiation fluxes over the Arctic Ocean: Sensitivity
601 to cloud optical properties, J. Climate, 5, 1267–1280, 1992.
602 Cziczo, D., Froyd, K., Gallavardin, S., Moehler, O., Benz, S., Saathoff, H., and Murphy, D.:
603 Deactivation of ice nuclei due to atmospherically relevant surface coatings, Environ.
604 Res. Lett., 4:044013, doi:10.1088/1748-9326/4/4/044013, 2009.
605 de Boer, G., Chapman, W., Kay, J. E., Medeiros, B., Shupe, M. D., Vavrus, S., and Walsh, J.:
606 A characterization of the present-day Arctic atmosphere in CCSM4, J. Climate, 25,
607 2676–2695, 2012.
608 DeMott, P. J.: An exploratory study of ice nucleation by soot aerosols, J. Appl. Meteorol.,
609 29(10), 1072–1079, 1990.
610 DeMott, P. J., Prenni, A. J., Liu, X., Petters, M. D., Twohy, C. H., Richardson, M. S.,
611 Eidhammer, T., Kreidenweis, S. M., and Rogers, D. C.: Predicting global atmospheric
612 ice nuclei distributions and their impacts on climate, P. Natl. Acad. Sci. USA, 107,
613 11217-11222, doi:10.1073/pnas.0910818107, 2010.
614 Dyer, A. J. and Hicks, B. B.: Flux-gradient relationships in the constant flux layer, Q. J. Roy.
615 Meteor. Soc., 96, 715–721, 1970.

Ervens, B., Feingold, G., Sulia, K., and Harrington, J.: The impact of microphysical parameters, ice nucleation mode, and habit growth on the ice/liquid partitioning in mixed-phase Arctic clouds, J. Geophys. Res., 116, D17205, doi:10.1029/2011JD015729, 2011.

Fan, J., Ovchinnikov, M., Comstock, J. M., McFarlane, S. A., and Khain, A.: Ice formation in Arctic mixed-phase clouds: Insights from a 3-D cloud-resolving model with size-resolved aerosol and cloud microphysics, J. Geophys. Res., 114, D04205, doi:10.1029/2008JD010782, 2009.

Feingold, G., Kreidenweis, S. M., Stevens, B., and Cotton, W. R.: Numerical simulation of stratocumulus processing of cloud condensation nuclei through collision-coalescence, J. Geophys. Res., 101, 21,391-21,402, 1996.

Fridlind, A. M., van Diedenhoven, B., Ackerman, A. S., Avramov, A., Mrowiec, A., Morrison, H., Zuidema, P., and Shupe, M. D.: A FIRE-ACE/SHEBA case study of mixed-phase Arctic boundary-layer clouds: Entrainment rate limitations on rapid primary ice nucleation processes, J. Atmos. Sci., 69, 365-389, doi:10.1175/JAS-D-11-052.1, 2012.

Hobbs, P. V. and Rangno A. L.: Microstructure of low and middle- level clouds over the Beaufort Sea, Q. J. Roy. Meteor. Soc., 124, 2035-2071, 1998.

Hoose, C. and Möhler, O.: Heterogeneous ice nucleation on atmospheric aerosols: a review of results from laboratory experiments, Atmos. Chem. Phys., 12, 9817-9854, doi:10.5194/acp-12-9817-2012, 2012.

Iacono, M. J., Delamere, J. S., Mlawer, E. J., Shephard, M. W., Clough, S. A., and Collins, W. D.: Radiative forcing by long-lived greenhouse gases: Calculations with the AER

639 Radiative transfer models, J. Geophys. Res., 113, D13103, doi:10.1029/2008JD009944,
640 2008.
641 Intrieri, J. M., Fairall, C. W., Shupe, M. D., Persson, P. O. G., Andreas, E., Guest, P. S., and
642 Moritz, R. E.: An annual cycle of Arctic surface cloud forcing at SHEBA, J. Geophys.
643 Res., 107, 8039, doi:10.1029/2000JC000439, 2002.
644 Kanji, Z., DeMott, P., Möhler, O., and Abbatt, J.: Results from the University of Toronto
645 continuous flow diffusion chamber at ICIS 2007: instrument intercomparison and ice
646 onsets for different aerosol types, Atmos. Chem. Phys., 11:31-41, doi:10.5194/acp-11-
647 31-2011, 2011.
648 Karlsson, J. and Svensson, G.: The simulation of Arctic clouds and their influence on the
649 winter surface temperature in present-day climate in the CMIP3 multi-model dataset,
650 Clim. Dynam., 36, 623–635, 2011.
651 Klein, S. A., McCoy, R., Morrison, H., Ackerman, A., Avramov, A., de Boer, G., Chen, M.,
652 Cole, J., DelGenio, A. D., Falk, M., Foster, M., Fridlind, A., Golaz, J.-C., Hashino, T.,
653 Harrington, J., Hoose, C., Khairoutdinov, M., Larson, V., Liu, X., Luo, Y., McFarquhar,
654 G., Menon, S., Neggers, R., Park, S., von Salzen, K., Schmidt, J. M., Sednev, I.,
655 Shipway, B., Shupe, M., Spangenberg, D., Sud, Y., Turner, D., Veron, D., Walker, G.,
656 Wang, Z., Wolf, A., Xie, S., Xu, K.-M., Yang, G., and Zhang, G.: Intercomparison of
657 model simulations of mixed-phase clouds observed during the ARM Mixed-Phase Arctic
658 Cloud Experiment. I: Single-layer cloud, Q. J. Roy. Meteor. Soc., 135, 979–1002, 2009.
659 Korolev, A.: Limitations of the Wegener–Bergeron–Findeisen mechanism in the evolution of
660 mixed-phase clouds, J. Atmos. Sci., 64, 3372–3375, doi:10.1175/JAS4035.1, 2007.

661 Korolev, A. and Sussman, B.: A technique for habit classification of cloud particles, J. Atmos.
662 Oceanic Technol., 17, 1048–1057, 2000.
663 Kulkarni, G., Fan, J., Comstock, J., Liu, X., and Ovchinnikov, M.: Laboratory measurements
664 and model sensitivity studies of dust deposition ice nucleation, Atmos. Chem. Phys.,
665 12:7295-7308, doi:10.5194/acp-12-7295-2012, 2012.
666 Levin, Z. and Yankofsky, S.: Contact versus immersion freezing of freely suspended droplets
667 by bacterial ice nuclei, J. Appl. Meteorol. Clim., 22, 1964-1966, 1983.
668 Lilly, D. K.: Models of cloud-topped mixed layers under a strong inversion, Q. J. Roy.
669 Meteor. Soc., 94, 292–309, 1968.
670 Lüönd, F., Stetzer, O., Welti, A., and Lohmann, U.: Experimental study on ice nucleation
671 ability of size selected kaolinite particles in the immersion mode, J. Geophys. Res.,
672 115:D14201, doi:10.1029/2009JD012959, 2010.
673 McFarquhar, G. M., Zhang, G., Poellot, M. R., Kok, G. L., McCoy, R., Tooman, T., Fridlind,
674 A., and Heymsfield, A. J.: Ice properties of single-layer stratocumulus during the Mixed-
675 Phase Arctic Cloud Experiment: 1. Observations, J. Geophys. Res., 112, D24201,
676 doi:10.1029/2007JD008633, 2007.
677 McFarquhar, G. M., Ghan, S., Verlinde, J., Korolev, A., Strapp, J. W., Schmid, B.,
678 Tomlinson, J. M., Wolde, M., Brooks, S. D., Cziczo, D., Dubey, M. K., Fan, J., Flynn,
679 C., Gultepe, I., Hubbe, J., Gilles, M. K., Laskin, A., Lawson, P., Leaitch, W. R., Liu, P.,
680 Liu, X., Lubin, D., Mazzoleni, C., Macdonald, A.-M., Moffet, R. C., Morrison, H.,
681 Ovchinnikov, M., Shupe, M. D., Turner, D. D., Xie, S., Zelenyuk, A., Bae, K., Freer, M.,
682 and Glen, A.: Indirect and Semi-Direct Aerosol Campaign (ISDAC): The Impact of

683 Arctic Aerosols on Clouds, B. Am. Meteorol. Soc., 92, 183–201,
684 doi:10.1175/2010BAMS2935.1, 2011.
685 Möhler, O., Bütuner, S., Linke, C., Schnaiter, M., Saathoff, H., Stetzer, O., Wagner, R.,
686 Krämer, M., Mangold, A., Ebert, V., and Schurath, U.: Effect of sulfuric acid coating on
687 heterogeneous ice nucleation by soot aerosol particles, J. Geophys. Res., 110:D11210,
688 doi: 10.1029/2004JD005169, 2005.
689 Möhler, O., Field, P., Connolly, P., Benz, S., Saathoff, H., Schnaiter, M., Wagner, R., Cotton,
690 R., Krämer, M., Mangold, A., and Heymsfield, A.: Efficiency of the deposition mode ice
691 nucleation on mineral dust particles, Atmos. Chem. Phys., 6:3007-3021,
692 doi:10.5194/acp-6-3007-2006, 2006.
693 Morrison, H. and Pinto, J. O.: Mesoscale modeling of springtime Arctic mixed-phase
694 stratiform clouds using a new two-moment bulk microphysics scheme, J. Atmos. Sci., 62,
695 3683-3704, 2005.
696 Morrison, H., Thompson, G., and Tatarskii, V.: Impact of cloud microphysics on the
697 development of trailing stratiform precipitation in a simulated squall line: Comparison of
698 one- and two-moment schemes, Mon. Wea. Rev., 137, 991-1007,
699 doi:10.1175/2008MWR2556.1, 2009.
700 Paulson, C. A.: The mathematical representation of wind speed and temperature profiles in
701 the unstable atmospheric surface layer, J. Appl. Meteor., 9, 857–861, 1970.
702 Persson, P. O. G.: Onset and end of the summer melt season over sea ice: Thermal structure
703 and surface energy perspective from SHEBA, Clim. Dynam., 39, 1349-1371,
704 doi:10.1007/s00382-011-1196-9, 2012.

705 Pinti, V., Marcolli, C., Zobrist, B., Hoyle, C., and Peter, T.: Ice nucleation efficiency of clay
706 minerals in the immersion mode, Atmos. Chem. Phys., 12:5859-5878, doi:10.5194/acp-
707 12-5859-2012, 2012.
708 Pruppacher, H. and Klett, J.: Microphysics of clouds and precipitation. Kluwer Academic
709 Publishers, 2nd edition, 1997.
710 Roberts, P. and Hallett, J.: A laboratory study of the ice nucleating properties of some
711 mineral particulates, Q. J. R. Meteorol. Soc., 94, 25 – 34, 1967.
712 Sandvik, A., Biryulina, M., Kvamsto, N., Stamnes, J., and Stamnes, K.: Observed and
713 simulated microphysical composition of Arctic clouds: Data properties and model
714 validation, J. Geophys. Res. 112, D05205, 2007.
715 Sedlar, J., Shupe, M. D., and Tjernström, M.: On the relationship between thermodynamic
716 structure, cloud top, and climate significance in the Arctic, J. Climate, 25, 2374–2393,
717 2012.
718 Sedlar, J., Tjernström, M., Mauritsen, T., Shupe, M. D., Brooks, I. M., Persson, P. O. G.,
719 Birch, C. E., and C. Leck, C.: A transitioning Arctic surface energy budget: The impacts
720 of solar zenith angle, surface albedo and cloud radiative forcing, Clim. Dynam., 37,
721 1643–1660, doi:10.1007/s00382-010-0937-5, 2011.
722 Serreze, M. C., Barrett, A. P., and Stroeve, J.: Recent changes in tropospheric water vapor
723 over the Arctic as assessed from radiosondes and atmospheric reanalyses. J. Geophys.
724 Res., 117, D10104, doi:10.1029/2011JD017421, 2012.
725 Sheridan, L. M., Harrington, J. Y., Lamb, D., and Sulia, K.: Influence of ice crystal aspect
726 ratio on the evolution of ice size spectra during vapor depositional growth, J. Atmos. Sci.,
727 66, 3732–3743, doi:10.1175/2009JAS3113.1, 2009.

728 Shupe, M. D.: A ground-based multiple remote-sensor cloud phase classifier, Geophys. Res.
729 Lett., 34, L2209, doi:10.1029/2007GL031008, 2007.
730 Shupe, M. D and J. M. Intrieri: Cloud radiative forcing of the Arctic surface: The influence
731 of cloud properties, surface albedo, and solar zenith angle, J. Climate, 17, 616-628, 2004.
732 Shupe, M. D, Matrosov, S. Y., and Uttal, T.: Arctic mixed phase cloud properties derived
733 from surface-based sensors at SHEBA, J. Atmos. Sci., 63, 697-811, 2006.
734 Shupe, M. D, Persson, P. O. G., Brooks, I. M., Tjernström, M., Sedlar, J., Mauritsen, T.,
735 Sjogren, S., and Leck, C.: Cloud and boundary layer interactions over the Arctic sea-ice
736 in late summer, Atmos. Chem. Phys., 13, 9379-9400, 2013.
737 Skamarock, W. C., Klemp, J. B., Dudhia, J., Gill, D. O., Barker, D. M., Duda, M. G., Huang,
738 X.-Y., Wang, W., and Powers, J. G.: A description of the Advanced Research WRF
739 version 3, NCAR Tech. Note NCAR/TN-475+STR, 113 pp., 2008.
740 Solomon, A., Morrison, H., Persson, P. O. G., Shupe, M. D., and Bao, J.-W.: Investigation of
741 microphysical parameterizations of snow and ice in Arctic clouds during M-PACE
742 through model-observation comparisons, Mon. Wea. Rev., 137, 3110-3128,
743 doi:10.1175/2009MWR2688.1, 2009.
744 Solomon, A., Shupe, M. D., Persson, P. O. G., and Morrison, H.: Moisture and dynamical
745 interactions maintaining decoupled Arctic mixed-phase stratocumulus in the presence of
746 a humidity inversion, Atmos. Chem. Phys, 11, 10127-10148, doi:10.5194/acp-11-10127-
747 2011, 2011.
748 Solomon, A., Shupe, M. D., Persson, P. O. G., Morrison, H., Yamaguchi, T., Caldwell, P. M.,
749 and de Boer, G.: The sensitivity of springtime Arctic mixed-phase stratocumulus clouds

to surface layer and cloud-top inversion layer moisture sources, J. Atmos. Sci., 71, 574-595, doi:10.1175/JAS-D-13-0179.1, 2014.

Tjernström, M., Sedlar, J., and Shupe, M. D.: How well do regional climate models reproduce radiation and clouds in the Arctic? An evaluation of ARCMIP simulations, J. Appl. Met. Clim., 47, 2405–2422, 2008.

Tjernström, M., C. Leck, C., Persson, P. O. G., Jensen, M. L., Oncley, S. P., and Targino, A.: The summertime Arctic atmosphere: Meteorological measurements during the Arctic Ocean Experiment 2001, B. Am. Meteorol. Soc., 85, 1305–1321, 2004.

Turner, D. D., Clough, S. A., Liljegren, J. C., Clothiaux, E. E., Cady-Pereira, K., and Gaustad, K. L.: Retrieving precipitable water vapor and liquid water path from Atmospheric Radiation Measurement (ARM) program's microwave radiometers, IEEE T. Geosci. Remote, 45, 3680–3690, 2007.

Verlinde, J., Harrington, J. Y., McFarquhar, G. M., et al.: The Mixed-Phase Arctic Cloud Experiment (M-PACE), B. Am. Meteorol. Soc., 88, 205–221, doi:10.1175/BAMS-88-2-205, 2007.

Walsh, J. E. and Chapman, W. L.: Arctic cloud-radiation temperature associations in observational data and atmospheric reanalyses, J. Climate, 11, 3030–3045, 1998.

Webb, E. K.: Profile relationships: The log-linear range, and extension to strong stability. Quart. J. Roy. Meteor. Soc., 96, 67–90, 1970.

Wise, M., Baustian, K., Koop, T., Freedman, M., Jensen, E., and Tolbert, M.: Depositional ice nucleation onto crystalline hydrated nacl particles: a new mechanism for ice formation in the troposphere, Atmos. Chem. Phys., 12:1121-1134, doi:10.5194/acp-12-1121-2012, 2012.

773 Yamaguchi, T. and Feingold, G.: Technical note: Large-eddy simulation of cloudy boundary
774 layer with the Advanced Research WRF model, J. Adv. Model. Earth Syst., 4, M09003,
775 doi:10.1029/2012MS000164, 2012.

776 **Figure Captions**

777 **Figure 1:** Sounding measured at 17:34 UTC 8 April 2008 at Barrow, Alaska (71.338N,
778 156.68W). Left) Water vapor mixing ratio (q_v), temperature (T), and potential temperature
779 (Theta), in units of g kg^{-1}, degrees Kelvin, and degrees Kelvin respectively. Right) Zonal
780 wind (U) and meridional wind (V), in units of m s^{-1}. Gray shading marks the extent of the
781 cloud layer. The dashed lines show the initial profiles used in the WRFLES experiments. The
782 dashed line overlaying water vapor mixing ratio is the initial profile for the total water
783 mixing ratio.

784 **Figure 2:** IN number concentration active at water saturation vs. temperature based on the
785 empirical relationship derived in DeMott et al. (2010) (blue line) used to initialize IN number
786 concentration in each bin. Black vertical lines indicate threshold temperatures for nucleation
787 in the 16 IN bins. IN increments between lines indicate the additional IN available for
788 nucleation at colder temperatures.

789 **Figure 3:** Sensitivity of ice water path to the parameter F in equation (2). Note the similar ice
790 water paths for F=4 and F=6 (total N_{IN} initial values 5.8 and 8.7 L^{-1}, respectively).

791 **Figure 4:** A,B,D) Sensitivity of LWP and IWP to snow density and fall speeds. LWP shown
792 with solid lines and IWP shown with dashed lines, in units of g m^{-2}. C) Fall speeds used in
793 sensitivity studies, in units of m s^{-1}. A) Sensitivity to reducing snow density from 100 kg m^{-3}
794 to 50 kg m^{-3} (red lines) using Control (CNT) fall speeds (red line in C). B) Sensitivity to
795 reducing snow fall speeds (green line in C) using Control snow density (red lines). D)
796 Sensitivity to increasing snow fall speeds (blue line in C) using Control snow density (red
797 lines).

798 **Figure 5:** Simulated ice particle number size distributions using in-cloud mass and number
799 concentrations. Ice water mixing ratio = 3e-4 g/kg, ice number concentration = 0.4/L, snow
800 water mixing ratio = 2.4e-2 g/kg, snow number concentration = 0.45/L.

801 **Figure 6:** (A) N_{IN} and (B) N_{ICE} averaged over 0.5 hours at hour 20, in units of L^{-1} hr^{-1}. Grey
802 shading indicates the extent of the cloud layer. Green dash lines indicate the top and bottom
803 of the mixed layer.

804 **Figure 7:** Time-height cross sections of horizontally-averaged (A) IN advection plus
805 subsidence, in units of $L^{-1}hour^{-1}$, (B) ice plus snow number concentration, in units of L^{-1}, (C)
806 water vapor mixing ratio, in units of g kg^{-1}, and (D) relative humidity with respect to ice, in
807 units of percent, from CNT simulation. Temperature, in units of °C, shown with black
808 contour lines in (B,C,D).

809 **Figure 8:** Control and NoRecycle time series for hours 6-40 (smoothed with 90 minute
810 running average). NoRecycle shown with red and black dashed lines. A) LWP (black) and
811 IWP (red), in units of g m^{-2}. B) Minimum horizontally-averaged temperature in the column,
812 in units of ^{o}C. C) Mixed-layer depth (blue), top height (red), and base height (black), in units
813 of km. D) N_{ICE} integrated over cloud layer (referred to as CL, red) and N_{IN} integrated over
814 subcloud layer (referred to as SubCL, black), in units of m L^{-1}(i.e., meters/liter).

815 **Figure 9:** Horizontally-averaged fluxes from Control and NoRecycle integrations for hours
816 6-40 (smoothed with 90 minute running average). NoRecycle shown with red and black
817 dashed lines. A) N_{ICE} flux at cloud base due to turbulence+subsidence+precipitation (red),
818 mixed-layer base due to turbulence+subsidence+precipitation (black), and due to activation
819 (multiplied by -1, blue), in units of m L^{-1} hr^{-1}. B) N_{IN} flux at cloud base due to turbulence

820 (red), N_{IN} flux due to sublimation (black), and precipitation of N_{ICE} at cloud base (multiplied
821 by -1, blue), in units of m L^{-1} hr^{-1}. C) N_{IN} entrainment at mixed-layer top (red) and base
822 (black), in units of m L^{-1} hr^{-1}.

823 **Figure 10:** Schematic of feedback loops that maintain ice production and the phase-
824 partitioning between cloud liquid and ice in an AMPS. Red colors denote N_{IN}. Blue colors
825 denote N_{ICE}. The size of the arrow indicates the relative magnitude of the flux. Vertical
826 profiles of N_{ICE}, N_{IN}, relative humidity, and temperature shown with thin blue, red, green, and
827 yellow lines, respectively.

828 **Figure 11:** A) LWP (black) and IWP (red), in units of g m^{-2}. (B) Downward surface
829 shortwave radiation and turbulent kinetic energy (TKE) at cloud base, in units of Wm^{-2} and
830 m^2s^{-2}, respectively. C) N_{ICE} in cloud layer (referred to as CL, red) and N_{IN} in subcloud layer
831 (referred to as SubCL, black), in units of m L^{-1}. (D) Total, turbulent, precipitation N_{ICE} flux at
832 cloud base (referred to as CL base, red, green, blue, respectively) and total N_{ICE} flux at
833 mixed-layer base (referred to as ML base, black), in units of m L^{-1} hr^{-1}, for the SW
834 integration for hours 16-76. Grey shading indicates hours with zero downwelling surface
835 shortwave radiation. E) N_{IN} entrainment at mixed-layer top (red) and base (black), in units of
836 m L^{-1} hr^{-1}. (F) N_{IN} flux at cloud base due to turbulence (red), N_{IN} flux due to sublimation
837 (black), and activation of N_{ICE} (blue), in units of m L^{-1} hr^{-1}.

838 **Figure 12:** A) Phase diagram of TKE at cloud base vs. N_{ICE} in the cloud layer starting at
839 peak shortwave hour 40, in units of m L^{-1} and m L^{-1} hr^{-1}, respectively. Colors show
840 sublimation in units of m L^{-1} hr^{-1}. H) 24-hour phase diagrams of sublimation vs. minimum
841 relative humidity in the subcloud layer starting at peak shortwave hour 40, in units of m L^{-1}

842 hr^{-1} and %, respectively. Colors show total N_{ICE} flux at cloud base, m L^{-1} hr^{-1}. Hours 42-47,
843 47-50, 50-56, and 57-62 indicated with green, blue, black, red arrows, respectively.
844 Minimum shortwave indicated with the moon symbol. Maximum shortwave indicated with
845 the sun symbol.

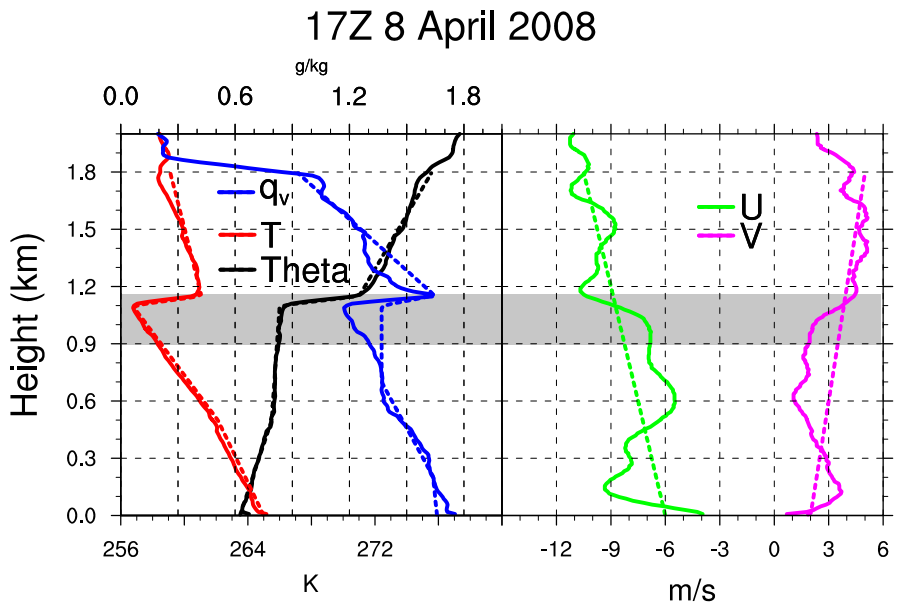

Figure 1: Sounding measured at 17:34 UTC 8 April 2008 at Barrow, Alaska (71.338N, 156.68W). Left) Water vapor mixing ratio (q_v), temperature (T), and potential temperature (Theta), in units of g kg^{-1}, degrees Kelvin, and degrees Kelvin respectively. Right) Zonal wind (U) and meridional wind (V), in units of m s^{-1}. Gray shading marks the extent of the cloud layer. The dashed lines show the initial profiles used in the WRFLES experiments. The dashed line overlaying water vapor mixing ratio is the initial profile for the total water mixing ratio.

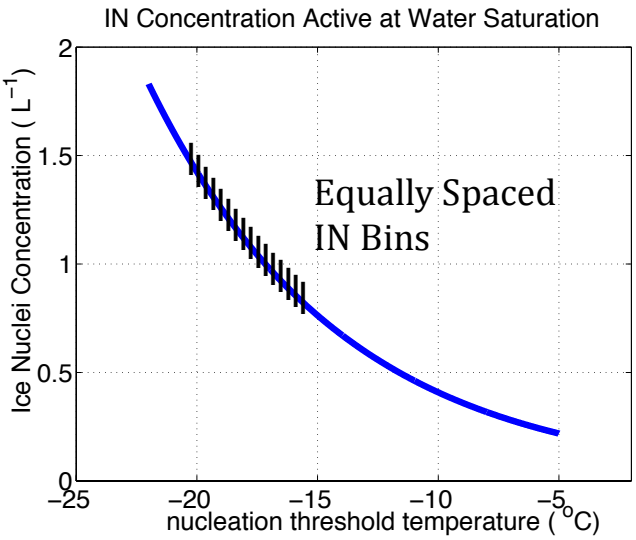

Figure 2: IN number concentration active at water saturation vs. temperature based on the empirical relationship derived in DeMott et al. (2010) (blue line) used to initialize IN number concentration in each bin. Black vertical lines indicate threshold temperatures for nucleation in the 16 IN bins. Note additional IN become available for nucleation at colder temperatures, such that, for example, at -20.2^{o}C (the coldest temperature in the Control simulation) the total number of IN available for activation is ~1.5 L^{-1}.

Amy Solomon 9/13/2015 1:57 PM
Deleted: IN increments between lines indicate the

Amy Solomon 9/13/2015 1:58 PM
Formatted: Superscript

Amy Solomon 9/13/2015 1:57 PM
Deleted: .

Amy Solomon 9/13/2015 2:00 PM
Formatted: Superscript

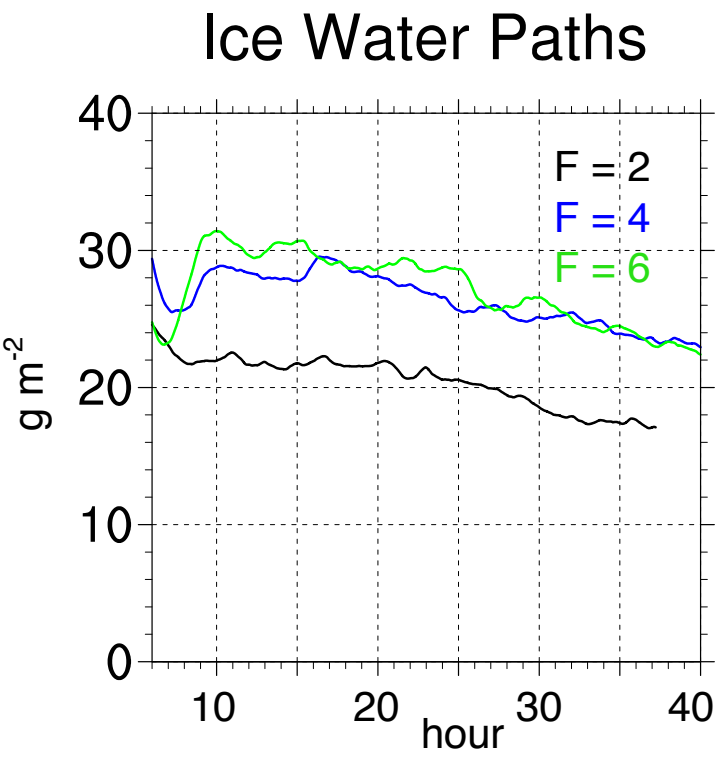

865

866 **Figure 3:** Sensitivity of ice water path to the parameter F in equation (2). Note the similar ice

867 water paths for F=4 and F=6 (total N_{IN} initial values of 5.8 and 8.7 L^{-1}, respectively).

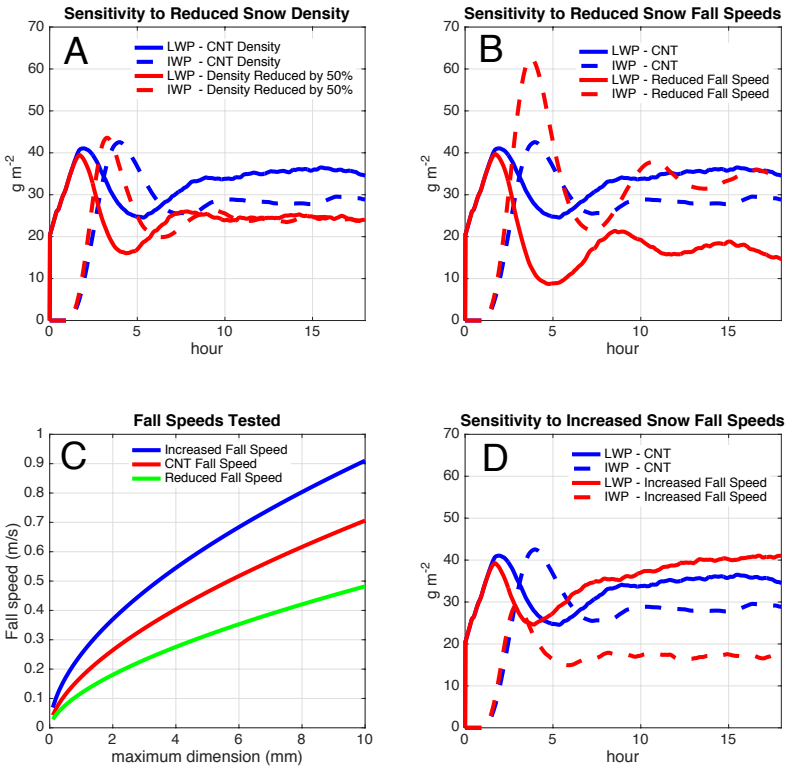

868

869 **Figure 4:** A,B,D) Sensitivity of LWP and IWP to snow density and fall speeds. LWP shown
870 with solid lines and IWP shown with dashed lines, in units of g m^{-2}. C) Fall speeds used in
871 sensitivity studies, in units of m s^{-1}. A) Sensitivity to reducing snow density from 100 kg m^{-3}
872 to 50 kg m^{-3} (red lines) using Control (CNT) fall speeds (red line in C). B) Sensitivity to
873 reducing snow fall speeds (green line in C) using Control snow density (red lines). D)
874 Sensitivity to increasing snow fall speeds (blue line in C) using Control snow density (red
875 lines).

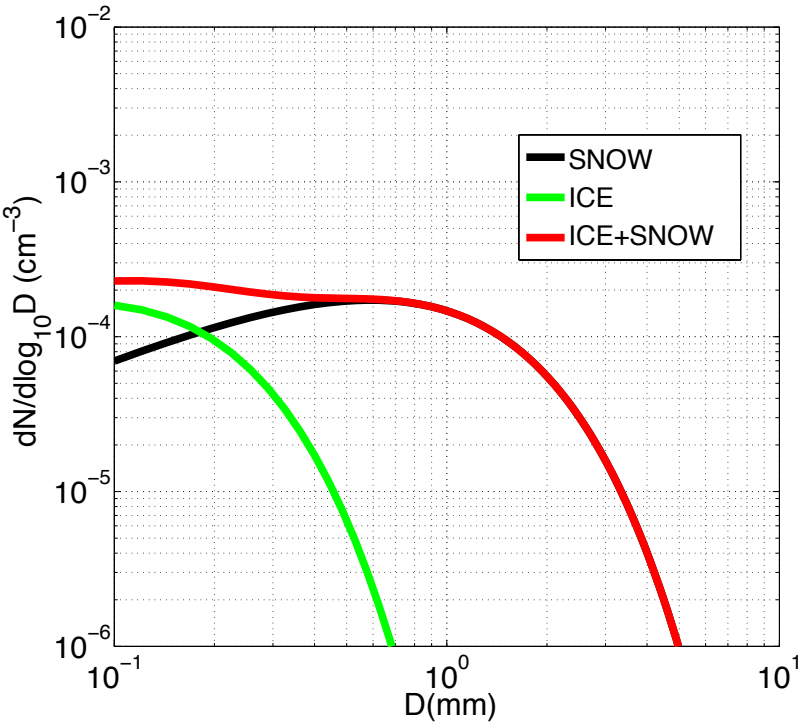

876

877 **Figure 5:** Simulated ice particle number size distributions using in-cloud mass and number

878 concentrations. Ice water mixing ratio = 3e-4 g/kg, ice number concentration = 0.4/L, snow

879 water mixing ratio = 2.4e-2 g/kg, snow number concentration = 0.45/L.

880

881

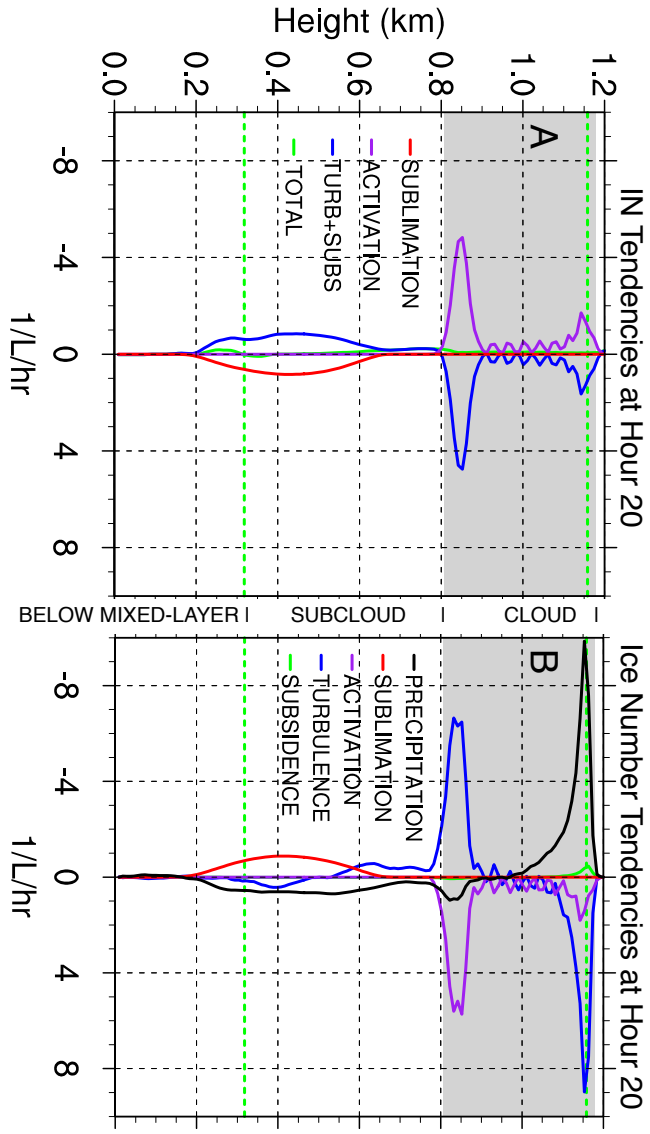

882 **Figure 6:** (A) N_{IN} and (B) N_{ICE} averaged over 0.5 hours at hour 20, in units of L^{-1} hr^{-1}. Grey
883 shading indicates the extent of the cloud layer. Green dash lines indicate the top and bottom
884 of the mixed layer.

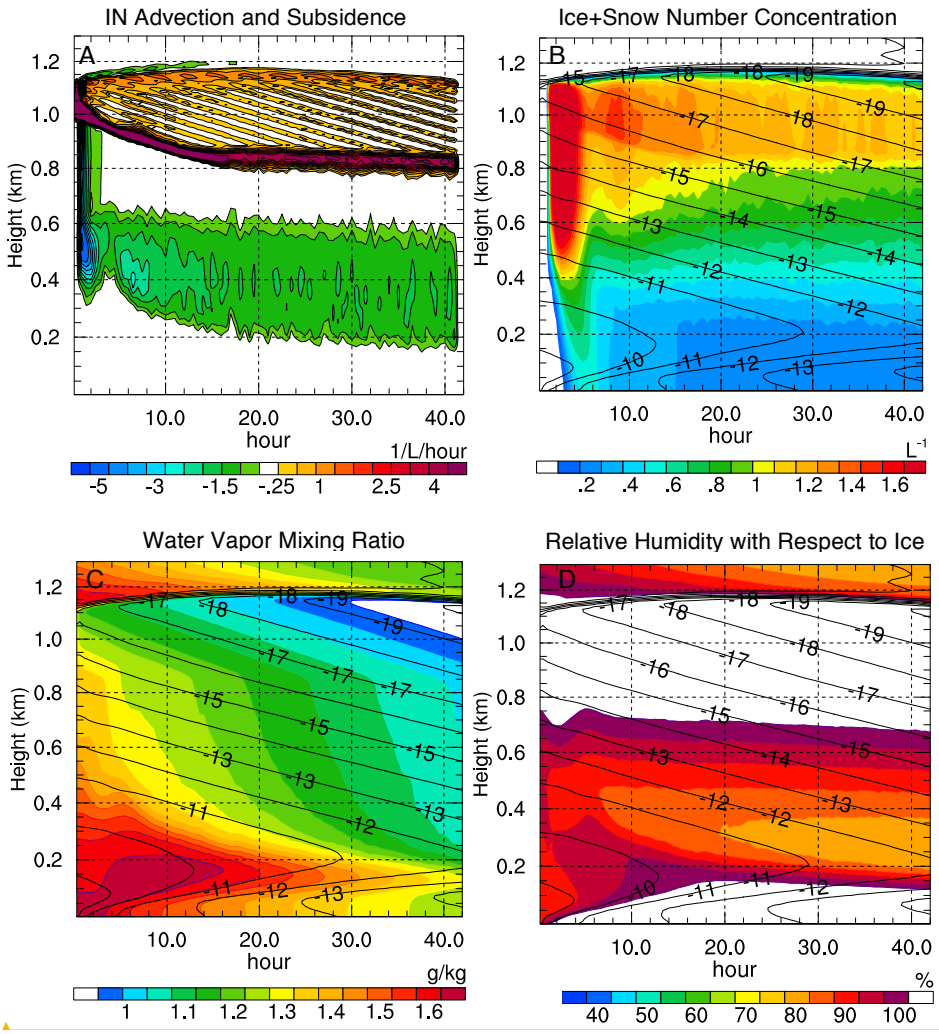

Unknown
Formatted: Font:Times New Roman, 12 pt, Font color: Red

Figure 7: Time-height cross sections of horizontally-averaged (A) IN advection plus subsidence, in units of $L^{-1}hour^{-1}$, (B) ice plus snow number concentration, in units of L^{-1}, (C) water vapor mixing ratio, in units of g kg^{-1}, and (D) relative humidity with respect to ice, in units of percent, from CNT simulation. Temperature, in units of °C, shown with black contour lines in (B,C,D).

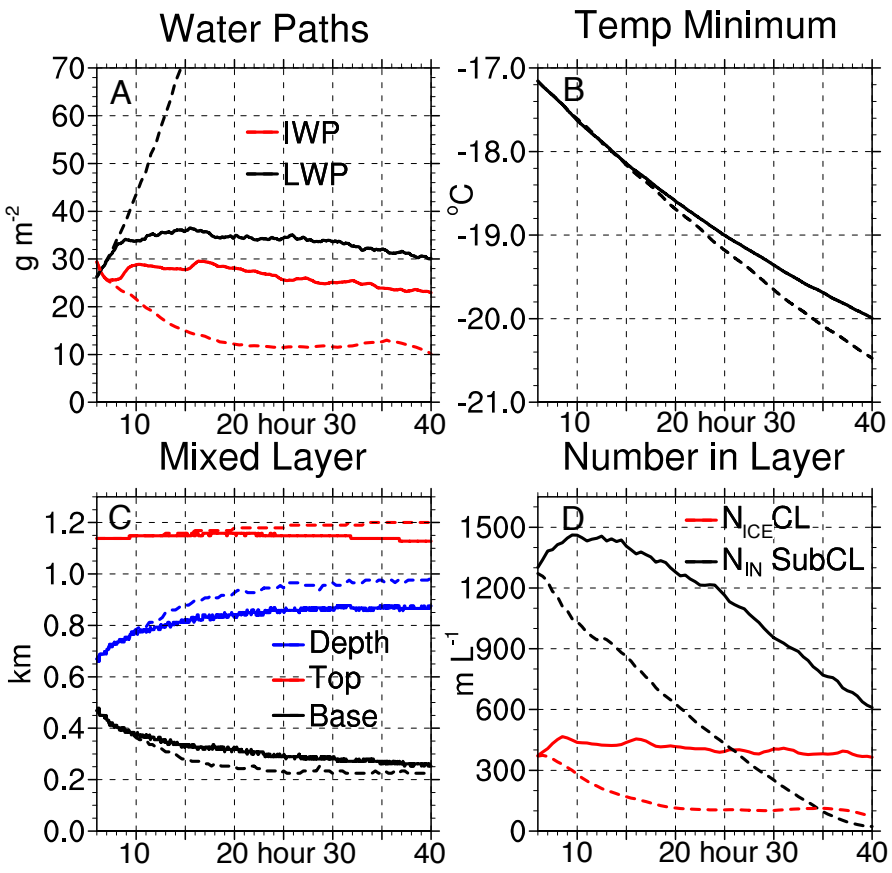

Figure 8: Control and NoRecycle time series for hours 6-40 (smoothed with 90 minute running average). NoRecycle shown with red and black dashed lines. A) LWP (black) and IWP (red), in units of g m^{-2}. B) Minimum horizontally-averaged temperature in the column, in units of ^{o}C. C) Mixed-layer depth (blue), top height (red), and base height (black), in units of km. D) N_{ICE} integrated over cloud layer (referred to as CL, red) and N_{IN} integrated over subcloud layer (referred to as SubCL, black), in units of m L^{-1}(i.e., meters/liter).

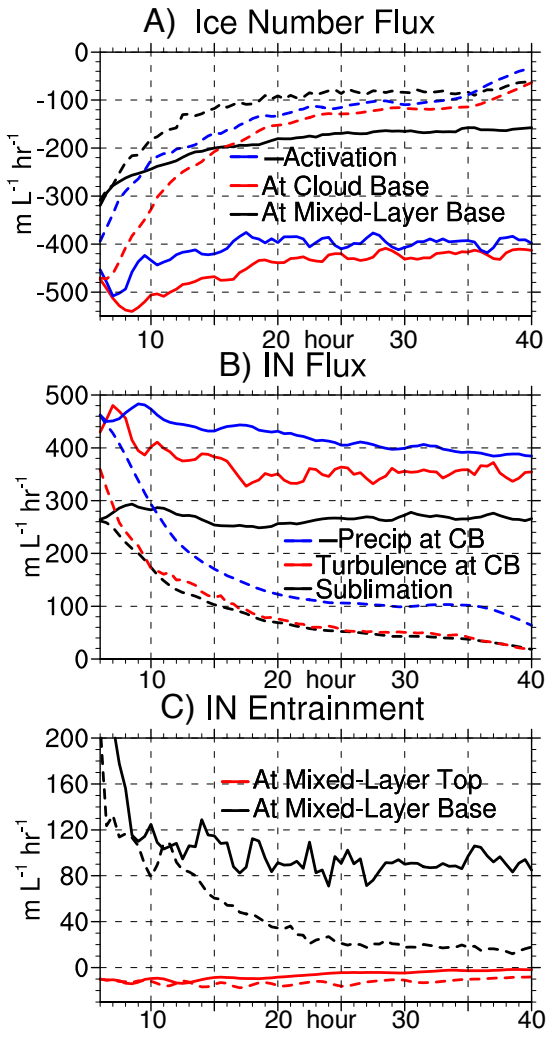

Figure 9: Horizontally-averaged fluxes from Control and NoRecycle integrations for hours 6-40 (smoothed with 90 minute running average). NoRecycle shown with dashed lines. A) N_{ICE} flux at cloud base due to turbulence+subsidence+precipitation (red), mixed-layer base due to turbulence+subsidence+precipitation (black), and due to activation (multiplied by -1, blue), in units of m L^{-1} hr^{-1}. B) N_{IN} flux at cloud base (indicated by CB in legend) due to turbulence (red), N_{IN} flux due to sublimation (black), and precipitation of N_{ICE} at cloud base (multiplied by -1, blue), in units of m L^{-1} hr^{-1}. C) N_{IN} entrainment at mixed-layer top (red) and base (black), in units of m L^{-1} hr^{-1}.

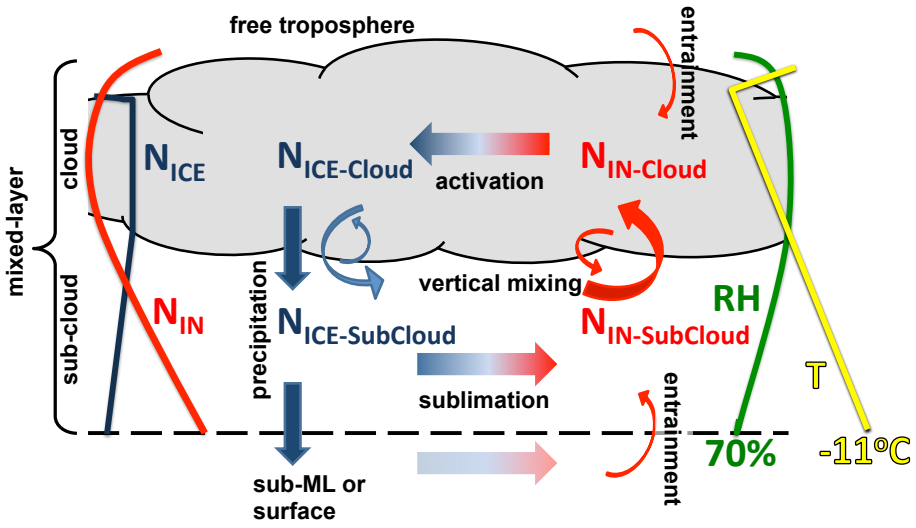

909

910 **Figure 10:** Schematic of feedback loops that maintain ice production and the phase-
911 partitioning between cloud liquid and ice in AMPS when recycling is allowed. Red colors
912 denote N_{IN}. Blue colors denote N_{ICE}. Vertical profiles of N_{ICE}, N_{IN}, relative humidity, and
913 temperature shown with thin blue, red, green, and yellow lines, respectively.

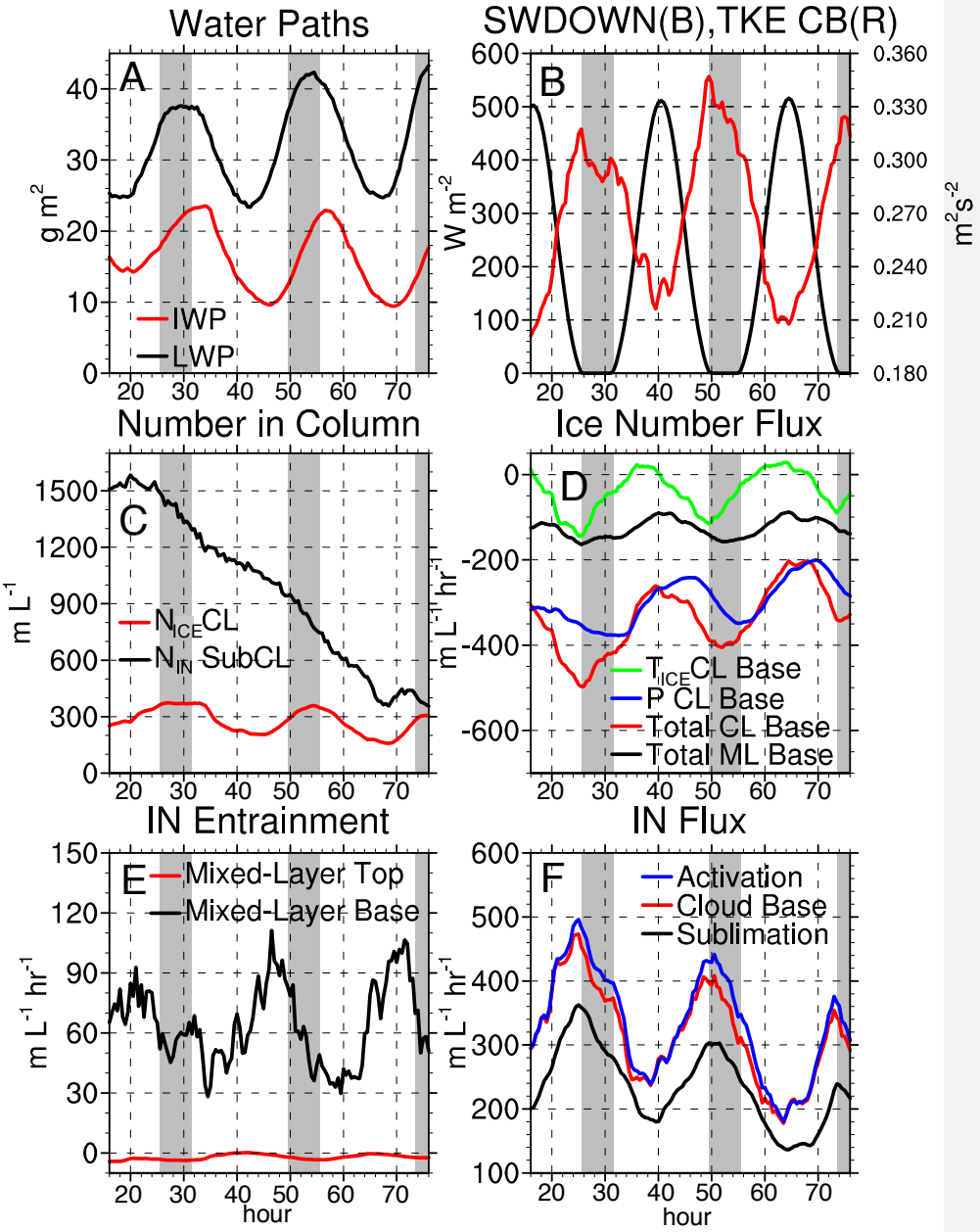

914

915 **Figure 11:** SW time series (see Figure captions).

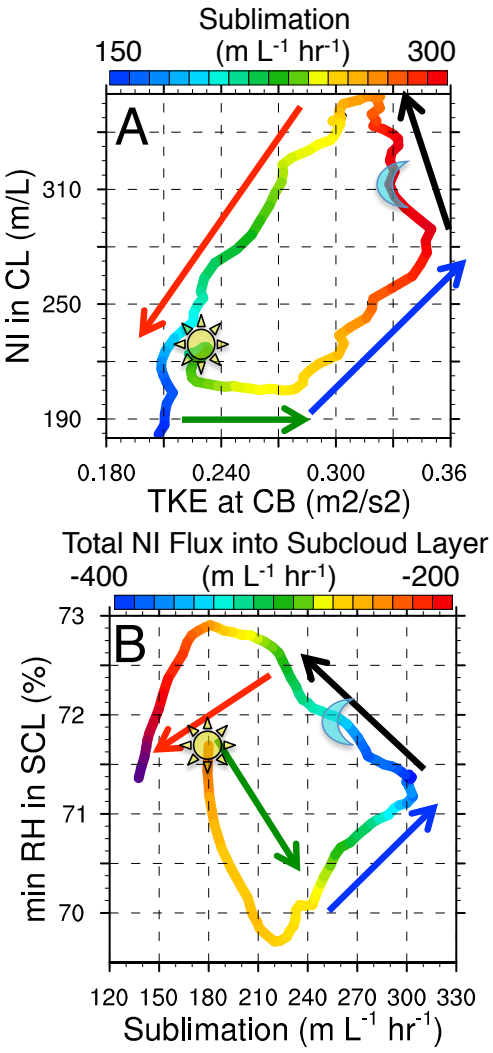

916

917 **Figure 12:** A) Phase diagram of TKE at cloud base vs. N_{ICE} in the cloud layer starting at
918 peak shortwave hour 40, in units of m L^{-1} and m L^{-1} hr^{-1}, respectively. Colors show
919 sublimation in units of m L^{-1} hr^{-1}. B) 24-hour phase diagrams of sublimation vs. minimum
920 relative humidity in the subcloud layer starting at peak shortwave hour 40, in units of m L^{-1}
921 hr^{-1} and %, respectively. Colors show total N_{ICE} flux at cloud base, m L^{-1} hr^{-1}. Hours 42-47,
922 47-50, 50-56, and 57-62 indicated with green, blue, black, red arrows, respectively.

923 Minimum shortwave indicated with the moon symbol. Maximum shortwave indicated with
924 the sun symbol.